AGU PUBLICATIONS

JGR

Journal of Geophysical Research: Atmospheres

RESEARCH ARTICLE

10.1002/2013JD021333

Key Points:
- Temperature has the dominant effect on influencing liquid cloud fraction
- Negative temporal and spatial correlations were found between SCF and RAFs
- Results are shown using spaceborne lidar observations for the first time

Correspondence to:
I. Tan,
ivy.tan@yale.edu

Citation:
Tan, I., T. Storelvmo, and Y.-S. Choi (2014), Spaceborne lidar observations of the ice-nucleating potential of dust, polluted dust and smoke aerosols in mixed-phase clouds, *J. Geophys. Res. Atmos.*, *119*, 6653–6665, doi:10.1002/2013JD021333.

Received 7 DEC 2013
Accepted 7 MAY 2014
Accepted article online 11 MAY 2014
Published online 5 JUN 2014

Spaceborne lidar observations of the ice-nucleating potential of dust, polluted dust, and smoke aerosols in mixed-phase clouds

Ivy Tan[1], Trude Storelvmo[1], and Yong-Sang Choi[2]

[1]Department of Geology and Geophysics, Yale University, New Haven, Connecticut, USA, [2]Department of Environmental Science and Engineering, Ewha Womans University, Seoul, South Korea

Abstract Previous laboratory studies and in situ measurements have shown that dust particles possess the ability to nucleate ice crystals, and smoke particles to some extent as well. Even with coatings of pollutants such as sulphate and nitrate on the surface of dust particles, it has been shown that polluted dust particles are still able to nucleate ice in the immersion, deposition, condensation, and contact freezing modes, albeit less efficiently than unpolluted dust. The ability of these aerosols to act as ice nuclei in the Earth's atmosphere has important implications for the Earth's radiative budget and hence global climate change. Here we determine the relationship between cloud thermodynamic phase and dust, polluted dust, and smoke aerosols individually by analyzing their vertical profiles over a ~5 year period obtained by NASA's spaceborne lidar, Cloud-Aerosol Lidar with Orthogonal Polarization. We found that when comparing the effects of temperature and aerosols, temperature appears to have the dominant influence on supercooled liquid cloud fraction. Nonetheless, we found that aerosols still appear to exert a strong influence on supercooled liquid cloud fraction as suggested by the existence of negative temporal and spatial correlations between supercooled liquid cloud fraction and frequencies of dust aerosols from around the world, at the −10°C, −15°C, −20°C, and −25°C isotherms. Although smoke aerosol frequencies were also found to be negatively correlated with supercooled liquid cloud fraction, their correlations are weaker in comparison to those between dust frequencies and supercooled liquid cloud fraction. For the first time, we show this based on observations from space, which lends support to previous studies that dust and potentially smoke aerosols can globally alter supercooled liquid cloud fraction. Our results suggest that the ice-nucleating ability of these aerosols may have an indirect climatic impact that goes beyond the regional scale, by influencing cloud thermodynamic phase globally.

1. Introduction

Mixed-phase clouds account for 20–30% of the global cloud coverage [*Ou et al.*, 2009] and have been observed in all seasons, under a variety of conditions, and in many locations worldwide [*Shupe et al.*, 2008]. The optical and microphysical properties of mixed-phase clouds and their ubiquity in the Earth's atmosphere are all factors that strongly influence the Earth's radiative budget and hydrological cycle. There are, however, large uncertainties associated with the way mixed-phase clouds affect global climate change due to both lack of observations and insufficient understanding of cloud microphysics; in particular, the various different modes of heterogeneous ice nucleation in mixed-phase clouds are complicated processes to understand. Heterogeneous ice nucleation can occur via the immersion, deposition, condensation, or contact modes, which lower the energy barrier required for ice nucleation in comparison to homogeneous (spontaneous) ice nucleation [*Vali*, 1985; *Pruppacher and Klett*, 1997]. The immersion freezing mechanism describes ice formation on an ice nucleus suspended in a supercooled liquid droplet. Deposition freezing occurs when supersaturated water vapor directly deposits on an ice nucleus. Condensation freezing, sometimes classified as immersion or deposition freezing, refers to ice nucleation that occurs when supersaturated water vapor condenses onto an ice nucleus which then freezes. Contact freezing occurs the instant an ice nucleus collides with a supercooled liquid droplet. Certain aerosols suspended in the Earth's atmosphere have long been known to impact clouds by acting as nuclei for ice crystal formation via the four aforementioned mechanisms, thereby altering the radiative properties and lifetimes of clouds [*Pruppacher and Klett*, 1997]. Ice-seeding aerosols, although rare, are therefore able to indirectly affect global climate via the way they alter cloud thermodynamic phase, which in turn affects cloud optical properties such as

optical depth, single-scattering albedo, and emissivity. Despite this, the current understanding of the impact of aerosols on ice formation in clouds is still in its infancy; identifying which aerosols are able to nucleate ice crystals and their relative efficiencies at nucleation are currently active areas of research [*Murray et al.*, 2012]. The radiative forcing resulting from aerosol-cloud interactions currently represents one of the largest, yet least understood forcings of the climate system [*Forster et al.*, 2007]. Aerosol impacts on cloud thermodynamic phase contribute significantly to the large uncertainty in radiative forcing [*Lohmann et al.*, 2010]. In this study, we focus on dust, polluted dust, and smoke aerosols, which have been shown by previous laboratory studies and in situ measurements from field campaigns to be discussed in what follows, to possess ice nucleation properties that can alter the proportion between supercooled liquid and ice in mixed-phase clouds.

The ice nucleation potential of mineral dust particles has been well-established for over half a century [*Isono et al.*, 1959]. The majority of these mineral dust particles originate from desert and semiarid regions. Once they get lofted into the atmosphere, they become one of the most efficient ice nuclei (IN) in the Earth's atmosphere at mixed-phase and cirrus cloud temperatures [*Hoose and Möhler*, 2012; *Murray et al.*, 2012]. A plethora of laboratory experiments consistently show that mineral dust aerosols are efficient IN below −15°C, displaying the ability to nucleate ice at relatively high temperatures and low ice supersaturations via several different modes of nucleation [see, e.g., *Field et al.*, 2006; *Koehler et al.*, 2010; *Niemand et al.*, 2012; *Connolly et al.*, 2009]. Furthermore, in situ studies by *DeMott et al.* [2003] and *Sassen et al.* [2003] also reported that mineral dust exhibits ice nucleation activity in the mixed-phase cloud temperature regime. Although there are no hard and fast rules, the properties that tend to make mineral dust particles efficient IN include their insolubility, relatively large and irregular shape (that therefore contain more "active sites" on which ice can form), ability to form chemical bonds with water, and lattice structure resembling that of ice [*Pruppacher and Klett*, 1997].

Dust particles inevitably get advected over long distances away from their sources, and when this occurs, they pick up coatings of sulphates, nitrates, and other electrolytes from polluted land masses [*Zhang and Carmichael*, 1999]. These substances coat the surface of dust particles, blocking off their so-called "active sites", thereby rendering them less efficient as IN [*Yang et al.*, 2011]. A wide variety of studies have lent support to the idea that pollutants decrease the ice-nucleating ability of IN, including dust. Laboratory studies have directly shown that coating surrogates for dust particles with sulphuric acid and ammonium nitrate significantly decreases the ice-nucleating ability of dust in the deposition and immersion freezing modes [*Cziczo et al.*, 2009] and immersion and condensation modes [*Eastwood et al.*, 2009] at mixed-phase cloud temperatures. In situ measurements taken during an arctic haze event during a field campaign also show that pollutants decrease the ice nucleation efficiency of IN [*Borys*, 1989]. Arctic haze is primarily composed of sulphate aerosols from distant pollution sources. When comparing the samples taken in situ from areas where arctic haze events took place and those taken from areas unaffected by distant pollution sources, *Borys* [1989] found that IN concentrations in the former areas were 1 to 3 orders of magnitude smaller than those in the latter areas. On the contrary, using samples of aluminum oxide, alumina-silicate, and iron oxide as surrogates for dust, *Archuleta et al.* [2005] found that coatings of sulphuric acid had not affected the ice-nucleating ability of aluminum oxide samples, had actually enhanced the ice-nucleating ability of iron oxide samples, but had decreased the ice-nucleating ability of alumina-silicates at cirrus cloud temperatures in the deposition freezing mode. In agreement with what *Archuleta et al.* [2005] had found with their aluminum oxide samples, *Knopf and Koop* [2006] found that sulphuric acid coatings on surrogates for dust particles had little to no effect on their ice-nucleating ability in the deposition freezing mode but at mixed-phase cloud temperatures.

While there is substantial evidence to support that mineral dust particles are efficient IN and several studies that support that coatings of pollutants decrease their ice nucleation efficiency, there is a lot more uncertainty associated with the ice nucleation efficiency of smoke particles, which are mainly by-products of incomplete combustion processes, such as biomass burning. Within this realm of uncertainty is the more fundamental question of whether smoke aerosols are able to function as IN to begin with. Previous studies have shown contradictory results. While some laboratory studies have reported that black carbon (BC), which is a primary constituent of smoke, can function as moderately efficient IN in the immersion mode [*DeMott*, 1990], contact mode [*Fornea et al.*, 2009], contact and/or deposition mode [*Gorbunov et al.*, 2001], and deposition, condensation, immersion, and contact modes [*Diehl and Mitra*, 1998], most studies have reported that BC particles are relatively poor IN, at least in the deposition mode [see, e.g., *Dymarska et al.*,

2006; *Friedman et al.*, 2011] in the mixed-phase cloud temperature regime. Still, in situ measurements from the lower troposphere have shown an enrichment of BC in ice crystal residuals, implying that BC particles may be able to function as IN in the Earth's atmosphere [*Cozic et al.*, 2008; *Targino et al.*, 2009]. It is important to note that while BC is a major component of smoke, organic matter on smoke particles may also be responsible for their ice nucleation efficiency [e.g., *Petters et al.*, 2009].

The aforementioned laboratory experiments and in situ measurements are some examples of studies that have shown that while there is currently no general consensus as to whether soot particles are able to function as IN at mixed-phase cloud temperatures, there is little to no doubt that unpolluted dust particles are able to function as efficient IN via the immersion, condensation, and deposition modes of nucleation at mixed-phase cloud temperatures. Like soot, previous laboratory experiments have not yet reached a consensus as to whether sulphate and nitrate coatings on dust particles decrease the ice nucleation efficiency of dust particles. Based on these studies, several different parameterizations of the ice nucleation efficiencies of these aerosols have been developed to numerically model their impact on the Earth's radiative budget. Model simulations have shown that dust and smoke aerosols acting as IN significantly affect the Earth's radiation budget. A numerical model sensitivity study by *Lohmann and Diehl* [2006] estimated that the aerosol indirect effect of ice nucleation by mineral dust in mixed-phase clouds contributes to a radiative forcing of up to 2.1 W m^{-2}. This value is more than a factor of 5 (with the opposite sign) larger than the value of −0.4 W m^{-2} due to the direct aerosol effect of dust on radiative forcing at the top of the atmosphere calculated using a global model by *Mahowald et al.* [2006]. Hence, the aerosol indirect effect of dust could play a more important role than its direct effect in the Earth's changing climate. Several modeling studies have also parameterized the influence of sulphuric acid on the efficiency of IN in the immersion, contact, and condensation modes of nucleation based on laboratory studies and have concluded that the "deactivation" effect of pollution coatings could potentially have a strong influence on mixed-phase clouds. The extent of the impact depends on how much sulphuric acid is required for the deactivation to occur [*Girard et al.*, 2005; *Storelvmo et al.*, 2008; *Lohmann and Hoose*, 2009]. The total industrial era climate forcing of BC is estimated to be +1.1 W m^{-2} with ∼90% uncertainty bounds of 0.11 W m^{-2} to 2.1 W m^{-2} [*Bond et al.*, 2013]. Of the total estimate of 1.1 W m^{-2}, up to 0.18 W m^{-2} with a large uncertainty range is derived from effects on cloud thermodynamic phase alone.

In addition to the numerous laboratory experiments, field campaigns, and modeling simulations that have studied the ice nucleation effects of dust and smoke aerosols on global climate, we wish to provide a study based on satellite observations. NASA's Cloud-Aerosol Lidar with Orthogonal Polarization (CALIOP) instrument aboard the Cloud-Aerosol Lidar and Infrared Pathfinder Satellite Observations (CALIPSO) satellite is able to vertically profile dust, polluted dust, and smoke aerosols and cloud thermodynamic phase on a global scale. We take advantage of its unique ability to distinguish between clouds and different aerosol types to determine the relationships between dust and smoke aerosols and "supercooled cloud fraction" (henceforth abbreviated as "SCF"), defined as the ratio of the frequency of supercooled liquid to the total frequency of supercooled liquid and ice (both randomly oriented and horizontally oriented) within a specified grid box size. Note that CALIOP does not have a separate "mixed-phase cloud" category (see the following section for details on the SCF calculations). Globally averaged SCFs calculated from CALIOP retrievals from 1 December 2007 to 31 December 2012 reveal that SCFs are consistently larger in the Southern Hemisphere at isotherms across the mixed-phase cloud temperature regime (Figure 1a, see section 2 for details on the data set and method of calculations). One possible explanation for this phenomenon is related to the obvious difference in land mass between the Northern and Southern Hemispheres. The Northern Hemisphere contains more land mass, from which efficient ice-nucleating aerosols originate. Such aerosols include mineral dust from desert and semiarid regions and smoke from anthropogenic activities such as biomass burning that can function as IN. Since the area above the ocean surface is relatively free of ice-nucleating aerosols at altitudes where mixed-phase clouds form [*Burrows et al.*, 2013], it is expected that average SCFs over land would be higher (Figure 1b). An abundance of aerosols in and transported away from source regions can have both direct and indirect, large-scale, and long-term climate effects. Our analysis of CALIOP retrievals suggests that the influence of dust, polluted dust, and smoke aerosols on ice nucleation in mixed-phase clouds is so pronounced that it can be seen from space at a spatial resolution typically used in global climate models.

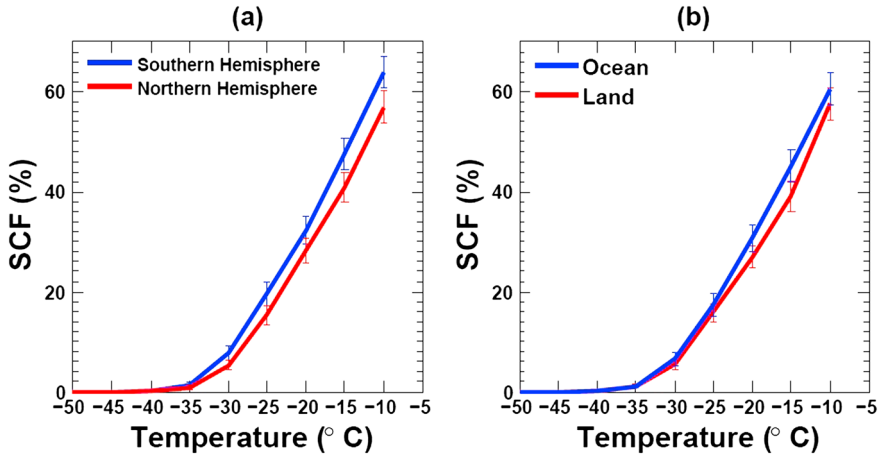

Figure 1. Comparison of supercooled cloud fractions (SCFs) averaged over (a) the Northern and Southern Hemispheres, and (b) over land and ocean, as a function of isotherm with standard error bars. The data are averaged from 1 December 2007 to 31 December 2012 and were obtained from CALIOP.

2. Calculations of Supercooled Cloud Fractions and Relative Aerosol Frequencies

We analyzed global (all longitudes, 82°S to 82°N) spaceborne lidar data of vertically-resolved profiles of cloud thermodynamic phase and *dust*, *polluted dust,* and *smoke* aerosols from NASA's CALIOP instrument from 1 December 2007 to 31 December 2012. Dust, polluted dust, and smoke are three of the six aerosol types that CALIOP is able to identify in the Earth's atmosphere. Dust primarily refers to mineral desert dust, polluted dust refers to dust mixed with biomass burning smoke and urban pollution, and smoke refers to aerosols emitted from biomass burning, composed primarily of soot and organic carbon. Launched on 28 April 2006, CALIOP is a dual-wavelength (532 nm, 1064 nm) nadir-viewing polarization lidar (the outgoing 532 nm pulses are linearly polarized with polarization purity >99%) that is mounted on the CALIPSO Sun-synchronous satellite that flies in the A-Train constellation at an altitude of 702 km. From the surface to 8.2 km, CALIOP has vertical and horizontal resolutions of 30 m and 333 m, respectively. Above 8.2 km in altitude, its vertical and horizontal resolutions are 60 m and 1000 m, respectively. The CALIOP "level 2" processing system consists of three modules, which are responsible for detecting layers with enhanced scattering, classifying the detected layers by type, and then performing extinction retrievals. In versions 3.01 and 3.02 of the CALIOP level 2 Vertical Feature Mask (VFM) product, once layers with enhanced scattering are detected, a set of algorithms is able to distinguish between aerosols and clouds based on five-dimensional probability distribution functions that depend on the mean attenuated backscatter coefficient at 532 nm, volume color ratio, depolarization, latitude, and height of the center of the layer (see *Liu et al.* [2009, 2010] for details on CALIOP's cloud-aerosol discrimination (CAD) algorithm). Furthermore, once layers are classified as being aerosol or cloud, six different aerosol types and cloud thermodynamic phase (either "water," "randomly-oriented ice" (ROI), or "horizontally-oriented ice" (HOI)) can be distinguished. Note that CALIOP was launched in April 2006, but only post-November 2007 data were analyzed for the reason that CALIOP's off-nadir-viewing angle was increased from 0.3° to 3° in November 2007, to reduce specular returns from clouds containing HOI crystals, which contribute to retrieval uncertainties [*Winker et al.*, 2009; *Hu et al.*, 2009]. Cloud thermodynamic phase is identified using temperature, height, and depolarization ratio [*Hu et al.*, 2009], while aerosol type is determined using a decision tree that takes into account information on volume depolarization ratio, attenuated backscatter signal, land surface type, and height with the goal of correctly estimating the lidar ratio to within 30% of its true value [*Omar et al.*, 2009]. Note that it is not possible to detect clouds and aerosols at the same place and time. Two more caveats should be borne in mind. First, since we are analyzing spaceborne lidar measurements of aerosols, there is no guarantee that every detected aerosol sample classified into a specific aerosol category excludes the presence of other aerosol types. As an example, a detected layer of dust may actually be a mixture of dust and smoke from biomass burning. In situ measurements have indeed shown that this may be the case for Saharan dust [*Hand et al.*, 2010]. Second, the aerosol subtyping scheme utilizes measured volume depolarization ratios and integrated attenuated backscatter signals to the extent possible; however, these two variables alone are not enough to fully constrain model selection. Surface type is therefore used and altitude as well since dust and

smoke are generally able to get lofted to higher altitudes [see *Omar et al.*, 2009, Figure 2]. The fact that the transport of aerosols is not explicitly taken into account in conjunction with the use of surface type in the subtyping scheme generally does not present a problem for dust since measured volume depolarization ratios allow for fairly accurate detection of dust particles, which have relatively large and distinct depolarization ratios; however, independent validation studies have shown that misclassifications of aerosol types do occur for polluted dust and more so for smoke. *Mielonen et al.* [2009], using a series of Sun photometers, and *Burton et al.* [2013], using an airborne high spectral resolution lidar (NASA Langley's High Spectral Resolution Lidar (HSRL)-1), have specifically validated CALIOP's subtyping scheme. The former study found that the Sun photometer and CALIOP's observations were in agreement for 91%, 53%, and 37% of the 277 days analyzed for dust, polluted dust, and smoke, respectively. The latter study found that 80% of CALIOP's dust layers were classified as either dust or a dusty mix but that only 35% of polluted dust layers and 13% of smoke layers agreed with their airborne lidar classifications. In contrast, a very recent validation study by *Kacenelenbogen et al.* [2014] also using HSRL-1, but targeted at assessing the ability of CALIOP to detect aerosols above clouds, found that CALIOP's most accurately classified aerosol type in agreement with classifications made with HSRL-1 was polluted dust. Their polluted dust category, however, was defined slightly differently from that of CALIOP. They found that CALIOP mostly misclassified the smoke, polluted continental, dust, and clean marine aerosol types. *Omar et al.* [2009] had also shown that use of surface type in the subtyping algorithm did not result in abrupt and artificial changes in aerosol type.

With its unique ability to identify and vertically resolve six different aerosol types and cloud thermodynamic phase around the globe, CALIOP is highly useful for better understanding the role of the interaction between aerosols and clouds. Our goal is to use data from CALIOP retrievals to examine the long-term relationship between SCFs and the frequency of occurrences of each of dust, polluted dust, and smoke aerosols from regions all around the globe as viewed from space. To achieve this, we employed versions 3.01 and 3.02 of the level 2 VFM to calculate SCFs and the newly released beta versions 1.00 and 1.30 of the level 3 Aerosol Profile Product (APP) under "all-sky" conditions to calculate aerosol frequencies. No significant differences between the "beta" and upcoming "provisional" version of the level 3 product are expected (D. Winker, personal communication, 2013). Note that the level 3 product is derived from the level 2 product. Several additional screening and filtering procedures have been applied to the level 2 product to obtain the level 3 product for quality assurance. The main screening and filtering processes involved making use of two quality flags as well as treatment of cloud edges. Retrievals with CAD scores classified as "no confidence" and extinction quality control flags indicating problematic retrievals were eliminated from the level 2 data set. Misclassification of clouds as aerosols by the CAD algorithm due to weak scattering of cloud edges in the upper troposphere above 4 km was treated by eliminating aerosol layers that were not adjacent to other aerosol layers [*Winker et al.*, 2013]. To avoid artifacts due to noise from scattering of sunlight, we analyzed nighttime CALIOP retrievals only, for both SCF and aerosol data, since they have a lower backscatter sensitivity threshold (see *Winker et al.* [2009] for a comprehensive overview and details on CALIPSO). Only data with medium and high confidence CAD scores were used for SCF calculations to minimize misclassifications of clouds as aerosols and vice versa. Regions between clouds and clear sky, where cloud contamination of aerosol retrievals is likely to occur, have been verified to decrease with the inclusion of increasing CAD confidence level scores [*Yang et al.*, 2011]. Although several screening and filtering processes were implemented in the data sets used in the current study, limitations such as misclassification of dust or smoke aerosols as clouds in dense layers of these aerosols near source regions may still occur due to their similar attenuated backscatter signals and color ratios and should be borne in mind as a caveat. Given this concern, the validity of CALIOP's CAD algorithm near strong source regions of dust and smoke has been extensively assessed using a variety of different techniques and instruments. A validation study using 1 month's worth of data has shown that these misclassifications are rare, occurring in < 1% of the cases studied for dust layers and even less frequently for smoke layers in the prescreened data set [*Liu et al.*, 2009]. Manual analysis of just under 300,000 features detected by CALIOP in 1 day has also suggested that the success rate of the CAD algorithm was in the neighborhood of 90% or better [*Liu et al.*, 2009]. Other independent studies specifically targeted to validate CALIOP's CAD algorithm near strong dust source regions include those by *Tesche et al.* [2013], who used ground-based lidar observations, *Pappalardo et al.* [2010], who used a series of Sun photometers, and *Omar et al.* [2010], who used in situ observations for their comparison. These studies had concluded that although CALIOP's CAD algorithm generally performed well, misclassifications of dense dust plumes as cloud did occur and that automatic classification of dense layers with intense backscatter detected in

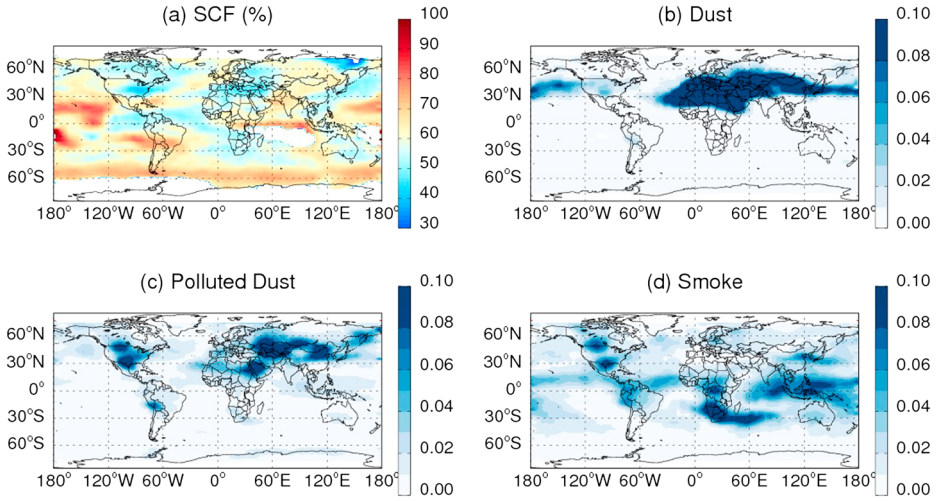

Figure 2. Global distribution of (a) supercooled cloud fractions (SCFs), (b) relative dust frequency, (c) relative polluted dust frequency, and (d) relative smoke frequency at the −10°C isotherm.

single-shot profiles automatically classified as cloud was largely responsible for the misclassifications. *Kim et al.* [2008], using a ground-based lidar, had also concluded that their observations were in good agreement with those of CALIOP for three different types of clear and cloudy conditions and had concluded that CALIOP's CAD algorithm provides reliable data.

SCFs were calculated following the methodology of *Choi et al.* [2010]. The number of liquid phase footprints divided by the total number of ice phase footprints (which includes HOI and ROI) were used to calculate SCF, i.e., SCF = liquid/(HOI + ROI), in 2° latitude by ~2.5° longitude grid boxes. Here a "footprint" refers to the circular area, each separated by the horizontal resolution of CALIOP, over which VFM flags are identified. Each footprint is separated by the horizontal resolution of CALIOP. SCFs were calculated at the mixed-phase cloud temperature range, −10°C to −30°C, in 5°C increments (for a total of five isotherms). CALIOP provides information on cloud top heights only for thick clouds and does not provide cloud top temperatures. We obtained cloud top temperatures by using National Centers for Environmental Prediction (NCEP)-Department of Energy (DOE) Reanalysis 2 air temperature and pressure data [*Kanamitsu et al.*, 2002] (at a resolution of 2.5°C longitude by ~2.5°C latitude resolution) in conjunction with CALIOP data. To ensure sufficient sample sizes, SCFs were calculated only in 10° latitude by 10° longitude grid boxes where the total number of liquid and ice footprints were ≥30.

Frequencies of dust, polluted dust, and smoke aerosols at each of the five isotherms were quantified as "relative aerosol frequencies" (RAFs). Aerosol frequencies were calculated differently from *Choi et al.* [2010]. Whereas daily values of cloud thermodynamic phase are provided by the level 2 VFM product, the level 3 APP data are provided as monthly totals of aerosol counts for each of the six aerosol types that CALIOP is able to detect. Due to the different format of the level 3 data, which does not resolve aerosol frequencies into daily averages, the temperatures of the aerosol layers were determined using a different method from that used for the SCF temperature calculations. Instead of using NCEP-DOE Reanalysis 2 data, the monthly mean temperatures, $\overline{T}$, in 2° latitude by 5° longitude grid boxes and their standard deviations provided by Goddard Global Modeling and Assimilation Office (GMAO) Reanalysis data in the CALIOP data set were considered. For grid boxes with a standard deviation of monthly mean temperature, $\sigma_T \leq 2.5$°C, the total monthly aerosol counts at these grid boxes are classified as having been detected at one (or more) of the five isotherms −10°C, −15°C, −20°C, −25°C, and −30°C if any of these isotherms fall in the range $\overline{T} \pm \sigma_T$. To allow for comparison among the three aerosol types we are interested in, RAFs were calculated by normalizing aerosol frequencies. Aerosol frequencies were divided by the maximum total monthly count (out of all aerosols) at each fixed isotherm. Thus, the maximum RAF is 1 and the minimum possible RAF is 0, indicating the region(s) with the most and least amount of aerosols at the isotherm in question, respectively.

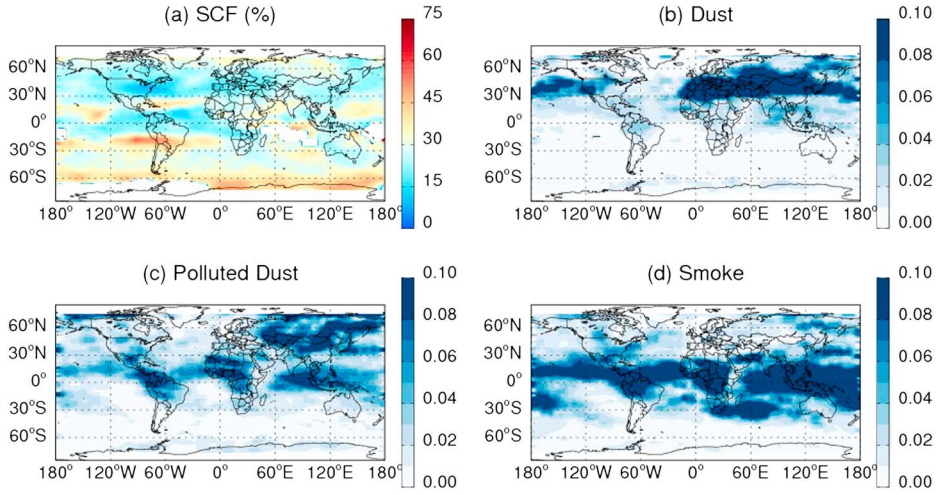

Figure 3. Global distribution of (a) supercooled cloud fractions (SCFs), (b) relative dust frequency, (c) relative polluted dust frequency, and (d) relative smoke frequency at the −20°C isotherm.

3. Global Distributions of Aerosols and Supercooled Cloud Fractions

The global distributions of SCFs and RAFs at three of the analyzed mixed-phase cloud isotherms, −10°C (Figure 2), −20°C (Figure 3), and −30°C (Figure 4) at 2° latitude by 5° longitude resolution show that SCF, dust, polluted dust, and smoke aerosols vary widely from region to region. By and large, regions with high RAFs correspond to regions with low SCF, although this is not the case for all regions. The large spatial variation in SCF is evidence that determining cloud phase based on temperature alone, a common practice in global models until recently, is crude and inaccurate. The distributions of RAFs are generally expected, bearing in mind that comparison between different isotherms is not meaningful since the RAFs are normalized relative to each fixed isotherm. The "dust belt" extending from the west coast of northern Africa, across the Middle East, central and South Asia to China is prominent at the −10°C, −20°C, and −30°C isotherms. Equally prominent is the transport of high frequencies of desert dust from the dust belt, across the Pacific Ocean to North America, where dust is less frequently found. Transport of Saharan dust by trade winds across the Atlantic to the USA and the Caribbean is most pronounced at the −10°C isotherm. At the −20°C isotherm, polluted dust aerosols are particularly conspicuous over the Amazon Forest, Central Africa, and Southeast Asia, where smoke from biomass burning due to agricultural activity and/or forest fires are common. Polluted dust from the Saharan Desert appears to derive from "clean" Saharan dust that

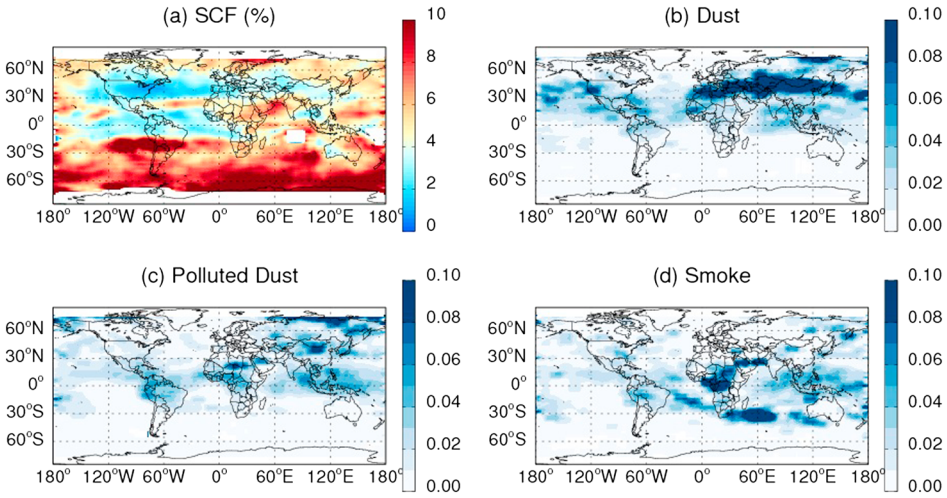

Figure 4. Global distribution of (a) supercooled cloud fractions (SCFs), (b) relative dust frequency, (c) relative polluted dust frequency, and (d) relative smoke frequency at the −30°C isotherm.

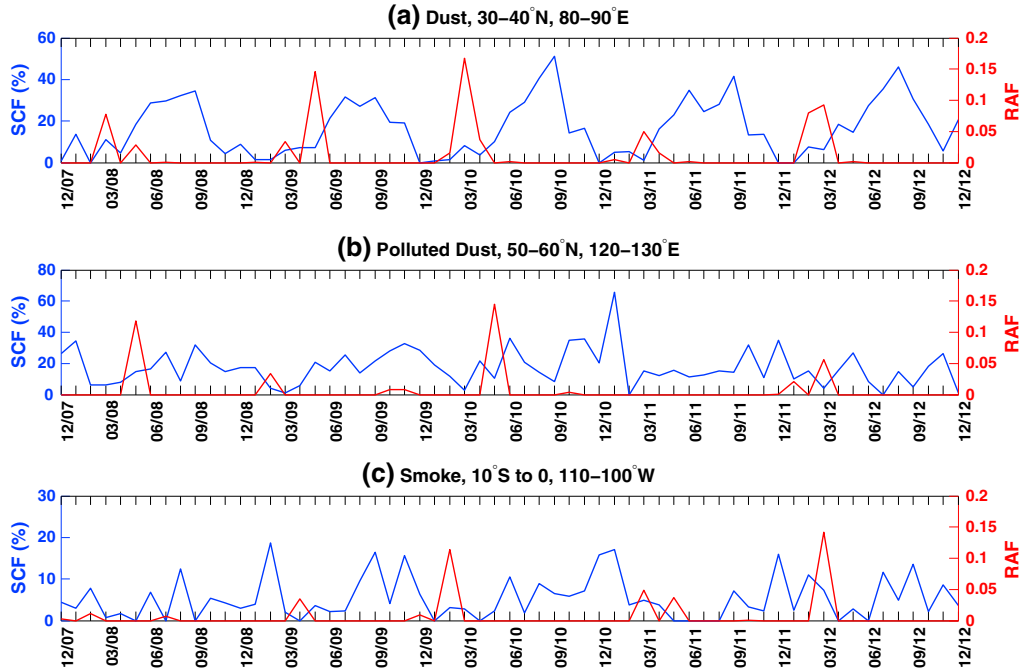

Figure 5. Time series plots of supercooled cloud fractions (SCFs) (blue) and (a) relative dust frequency in the Taklamakan Desert at the −20°C isotherm (red), (b) relative polluted dust frequency in Far East Russia at the −20°C isotherm (red), and (c) relative smoke frequency off the coast of the Amazon Forest at the −30°C isotherm (red).

has been influenced by downwind-blown smoke from Southeast Asia, at all of the isotherms. Smoke can be seen over regions of active biomass burning, such as South and Central Africa, as well as Southeast Asia, at all three isotherms, and in Central America at the −20°C isotherm. High frequencies of all three aerosols occur over both land and ocean; however, those over land are higher in frequency since they are source regions. Aerosols over the ocean surface are lower in frequency since they are located downwind of the source regions on land. It is worth pointing out that the Southern Ocean is consistently virtually free of dust, polluted dust and smoke aerosols.

4. Temporal and Spatial Correlations Between Aerosols and Supercooled Cloud Fractions

To better understand and quantify the relationship between each of the aerosols and cloud thermodynamic phase over the ~5 year period, temporal correlations between monthly averages of SCF and monthly averages of each of the RAFs were performed. Due to the 16-day orbit of CALIOP, the horizontal resolution of the data set was reduced to 10° latitude by 10° longitude grid boxes to avoid the issue of a sparse data set when performing the temporal correlations. Time series plots of SCF and RAF data in selected regions are displayed in Figure 5. At the −20°C isotherm, high frequencies of dust in the Taklamakan Desert peak in months coinciding with months when SCFs are at minima (Figure 5a). Similarly, at the same isotherm, high frequencies of polluted dust aerosols in Far East Russia peak in months when SCF is low (Figure 5b). The polluted dust aerosols are presumably dust particles originating from the Taklamakan Desert and Gobi Desert regions that are then picked up by the westerlies and aged with coatings of pollutants as they traveled downwind. The time series data of monthly averaged relative smoke frequencies were selected over a region off the coast of the Amazon Forest, where biomass burning frequently occurs, at the −30°C isotherm, a temperature at which BC found in smoke is more efficient at ice nucleation [*Murray et al.*, 2012] (Figure 5c). As in the case of dust and polluted dust, months with high relative smoke frequencies tend to occur at months when SCFs are relatively low. Therefore, these regions show that negative temporal correlations exist between SCF and each of the three aerosols.

Next, we show that spatial correlations also exist between SCF and the RAFs. Regions with temporal correlations between SCFs and RAFs significant at the 95% confidence level were grouped into individually specified RAF ranges (which will henceforth be referred to as "relative aerosol frequency (RAF) bins"), in order

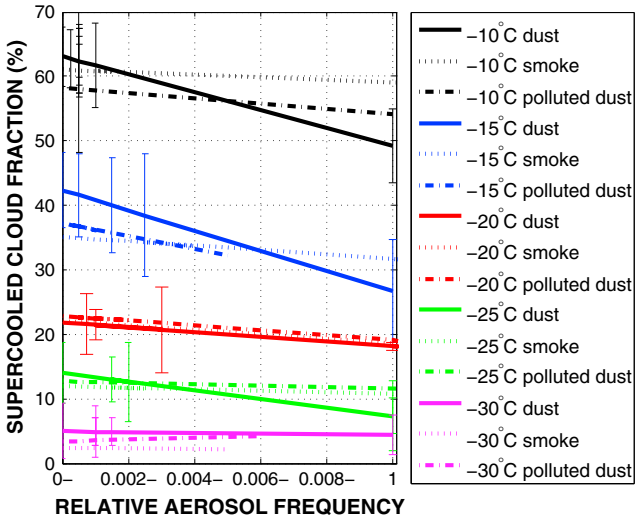

Figure 6. Spatial correlations between median supercooled cloud fractions (SCFs) and relative aerosol frequencies (RAFs) at five mixed-phase cloud isotherms, using only data from 10° latitude by 10° longitude regions temporally correlated at the 95% confidence level. Note the larger range of the bin containing RAFs extending from 0.008 to 1. Normalizing the aerosol frequencies by the maximum value at each isotherm resulted in many smaller RAFs and fewer but still, several larger RAFs. The larger RAFs were grouped with the next smallest bin, resulting in the bin extending from 0.008 to 1.

to perform spatial correlations between SCFs and RAFs. To minimize erroneous spatial correlations, only regions with temporal correlations significant at the 95% confidence level were considered when determining the spatial correlations between each of the RAFs and SCF. Figure 6 shows a least squares linear regression fitted through the median SCFs associated with the SCF distributions for all mixed-phase cloud isotherms relevant to our analysis. The spatial correlation coefficients for the least squares linear regressions for each of the distributions at each isotherm are summarized in Table 1. Spatial correlation coefficients computed using prescreened RAF data (versions 3.01 and 3.02 of the level 2 VFM data) following the method of *Choi et al.* [2010] are displayed in parentheses in Table 1. The standard error bars associated with the polluted dust and smoke data are similar in magnitude to those for the dust data and have been omitted from Figure 6 for the sake of clarity. The use of RAF bins in our analysis is twofold; first, it reflects the aforementioned uncertainties associated with the CALIOP retrievals used to calculate RAFs; second, focusing on the median SCF of each bin effectively eliminates the large fluctuations in SCF seen in Figure 5. The RAF bin sizes are different for each aerosol and isotherm that was analyzed but are displayed as five bins, for the sake of clarity. The bins were chosen such that the distribution of SCFs within each bin has an optimal number of data points; bins that are too large will lower confidence level of the linear regression; however, bins that are too small will not sufficiently eliminate the fluctuations in SCFs.

Only the signs of the slopes of the linear regressions, and not their magnitudes, are of interest in the present study. From Figure 6, it is clear that between the effects of temperature and aerosols, temperature has the dominant influence on SCFs but that at a fixed temperature, each of the three aerosols exerts an influence on SCF, shown by the negative slopes. It is evident that in all of the regions with high frequencies of dust, polluted dust, and smoke, the corresponding SCFs as calculated using CALIOP retrievals are relatively low, demonstrating that SCF and RAFs are not only temporally correlated, as Figure 5 shows, but also spatially correlated. Conversely, regions with little to no dust or smoke aerosols have relatively high SCF values. Given the finding from numerous previous laboratory studies and field campaigns that have suggested that these aerosol types act as IN in the free troposphere, our results suggest (but do not prove) that the presence of these aerosols acting as IN is actively lowering the SCFs by increasing the ratio of ice crystals to liquid droplets in these regions. Our results also suggest that the absence of dust and smoke aerosols is contributing to the relatively higher SCFs, which is particularly pronounced over the Southern Ocean.

Table 1. Spatial Correlation Coefficients for the Linear Regressions in Figure 6[a]

Isotherm (°C)	Dust	Polluted Dust	Smoke
−10	0.48 (0.98)	0.25 (0.84)	0.24 (0.71)
−15	0.75 (0.85)	0.86 (0.56)	0.31 (0.79)
−20	0.76 (0.96)	0.53 (0.86)	0.47 (0.57)
−25	0.85 (0.94)	0.58 (0.97)	0.35 (0.83)
−30	0.012 (0.98)	0.082 (0.84)	0.31 (0.71)

[a]Spatial correlation coefficients based on prescreened data (versions 3.01 and 3.02 of the level 2 VFM product), where RAFs were calculated differently, using NCEP-DOE Reanalysis 2 data, instead of Goddard GMAO Reanalysis data, to obtain the isotherms, following the method of *Choi et al.* [2010], are in parentheses.

Both the temporal and spatial correlations between SCFs and dust, polluted dust, and smoke frequencies at mixed-phase cloud temperatures shown in Figures 5 and 6, respectively, along with Table 1, substantiate observations from the maps displayed in Figures 2–4. From regions that are temporally correlated at the 95% confidence level over a period of ~5 years, CALIOP retrievals show that the median SCFs are negatively correlated with increasing aerosol frequencies, in 10° latitude by 10° longitude grid boxes. The size of each grid box is rather large and cannot be helped due to the 16-day orbit of CALIOP; however, we emphasize that we are making the statistical argument that over a long time scale and over particular regions, the fact that RAFs and SCFs are negatively temporally correlated at the 95% confidence level over a 61 month interval implies that it is very unlikely that the correlations happened by chance. Dust and smoke aerosols are likely influencing the decreased SCFs in the regions these aerosols are found, as detected by CALIOP. The spatial correlation coefficients at the −15°C, −20°C, and −25°C isotherms (Table 1) for dust and polluted dust are statistically significant; however, those for smoke aerosols are not statistically significant. These results suggest that while dust and polluted dust aerosols are likely playing a role in ice nucleation in the Earth's atmosphere, no such suggestion can be made for smoke aerosols with confidence. Although smoke aerosols are generally not considered to be efficient IN, their shear abundance in the Earth's atmosphere, mostly as a result of increasing anthropogenic activities, may be able to enhance their probability of nucleating ice crystals [*Murray et al.*, 2012].

At the other two mixed-phase cloud isotherms of −10°C and −30°C, the spatial correlation coefficients are much lower, which is expected, and the slope is relatively horizontal, and slightly positive at the −30°C isotherm. Dust aerosols are known to be some of the most efficient IN present in the Earth's atmosphere but are only active at relatively cold temperatures [*Hoose and Möhler*, 2012; *Murray et al.*, 2012]. Bacteria are considered to be more important for ice nucleation at higher mixed-phase cloud temperatures (~ −10°C) [*Murray et al.*, 2012; *Sesartic et al.*, 2012]. The relatively horizontal and slightly positive slopes and low correlation coefficients at −30°C for all the aerosols we examined can be explained by the low temperature. This temperature is approaching the threshold of approximately −38°C, where spontaneous freezing of supercooled liquid occurs. The proximity of −30°C to the homogeneous freezing threshold also explains the decreasing standard deviation of SCF with decreasing temperature. The striking difference in the correlation coefficients between the screened and prescreened data at the −30°C isotherm can be explained by the fact that the screening process predominantly affected optically thin cirrus clouds above 6 km that were misclassified as aerosol layers [*Winker et al.*, 2013].

Although we cannot rule out the possibility of small-scale processes that are unrelated to ice nucleation by dust, polluted dust, and smoke aerosols to explain the negative temporal and spatial correlations, we obtained between SCFs and dust, polluted dust, and smoke aerosols the spatial correlation coefficients between mean SCF and relative dust, and polluted dust frequencies at the −15°C, −20°C, and −25°C isotherms are statistically significant. The implication of our results is that dust aerosols (in their clean and polluted forms) are acting as IN over certain regions and therefore may be responsible for the low SCFs found in those regions, although temperature has a stronger influence on SCFs in comparison. The effect of aerosols on SCF is large enough to be seen on a global scale from space. The reader should be aware that although CALIOP's CAD algorithm and aerosol subtyping scheme have been independently validated on numerous occasions using a variety of different techniques and instruments, misclassifications, especially those that occur near strong source regions of dust and smoke, could potentially lead to weakened temporal and spatial correlations between the SCFs and RAFs.

5. Summary and Conclusions

Analysis of vertical profiles of cloud thermodynamic phase and aerosols obtained from NASA's spaceborne CALIOP instrument has shown that the influence of dust and possibly smoke aerosols on cloud thermodynamic phase may impact climate on a global spatial scale and multiannual time scale. Versions 3.01 and 3.02 of level 2 CALIOP data and NCEP-DOE Reanalysis 2 data were used to calculate supercooled cloud fractions (SCFs). Version 1.00 of level 3 CALIOP data was used to calculate relative aerosol frequencies (RAFs). The distributions of dust, polluted dust, and smoke aerosols were quantified at five equally spaced mixed-phase cloud isotherms by counting their frequency of occurrences within 2° latitude by 5° longitude grid boxes at each isotherm. These frequencies were normalized by the maximum monthly average value at each isotherm to get the RAF to allow for comparison among the three aerosols at a fixed isotherm. Similarly, the

SCFs at each isotherm were calculated by dividing the frequency of liquid detected by the summation of liquid droplets and ice (both horizontally and randomly oriented) in 2° latitude by 5° longitude grid boxes. We quantified the relationship between each of the aerosols and cloud thermodynamic phase by performing temporal correlations of each of the RAFs with SCF in 10° latitude by 10° longitude grid boxes. The regions with temporal correlations significant at the 95% confidence level were then classified into one of a varying numbers of aerosol frequency bins, each range containing a distribution of SCFs. Least squares linear regressions were then fitted to the median SCFs of each of the aerosol distributions.

We found negative spatial correlations between each of the RAFs and median SCFs for the least squares linear regressions at −10°C, −15°C, −20°C, and −25°C, although the negative correlations are weaker for polluted dust and smoke. At −30°C, the slopes were relatively horizontal and slightly positive; the proximity of this temperature to that at which spontaneous freezing occurs may explain the low and little varying SCFs. The negative slopes for dust and polluted dust aerosols are statistically significant at the −10°C, −15°C, −20°C, and −25°C isotherms; however, the negative slopes for smoke aerosols are not statistically significant. This suggests that the presence of dust aerosols (in their clean and polluted forms) in regions around the globe at mixed-phase cloud temperatures decreases SCFs in those regions, presumably because these aerosols are nucleating ice crystals. Although we cannot rule out the possibility of atmospheric processes unrelated to ice nucleation by dust and polluted dust to explain the decrease in SCFs found in those regions, our results do show that correlations between median SCF and dust and polluted dust frequencies over a ~5 year time scale are unlikely to have occurred by chance. The negative correlations between median SCF and relative smoke frequencies are not statistically significant across the mixed-phase cloud temperature regime, and we are therefore not able to make the same suggestion for smoke aerosols. Our results show that although the three aerosol types studied exhibit weaker influences on SCF in comparison to temperature, the influences of dust and perhaps smoke aerosols on SCFs are nevertheless important, supporting previous microphysical laboratory studies on the ice-nucleating ability of dust and smoke particles. Finally, as a word of caution, although numerous independent validation studies show that CALIOP's CAD algorithm and aerosol subtyping scheme generally perform well, misclassifications do occur, especially in and around strong sources regions of dust and smoke. These misclassifications could potentially result in a weakening of the negative temporal and spatial correlations between the SCFs and RAFs.

Acknowledgments

CALIOP data are available online at the NASA Langley Atmospheric Sciences Data Center website (https://eosweb.larc.nasa.gov/order-data). NCEP-DOE Reanalysis 2 data are also available online at http://www.esrl.noaa.gov/psd/data/gridded/data.ncep.reanalysis2.pressure.html. Yong-Sang Choi was supported by the Korean Ministry of Environment as the Eco-technopia 21 project (201200016003) and the National Research Foundation of Korea (NRF) grant funded by the Korea government (MSIP) (2009-0083527). The authors wish to thank David M. Winker for his invaluable advice on usage of CALIOP products and Hye-Ryun Oh from Seoul National University for her assistance in data handling at the initial stages of our work.

References

Archuleta, C. M., P. J. DeMott, and S. M. Kreidenweis (2005), Ice nucleation by surrogates for atmospheric mineral dust and mineral dust/sulfate particles at cirrus temperatures, *Atmos. Chem. Phys.*, *5*(10), 2617–2634, doi:10.5194/acp-5-2617-2005.

Bond, T. C., et al. (2013), Bounding the role of black carbon in the climate system: A scientific assessment, *J. Geophys. Res. Atmos.*, *118*, 5380–5552, doi:10.1002/jgrd.50171.

Borys, R. D. (1989), Studies of ice nucleation by Arctic aerosol on AGASP-II, *J. Atmos. Chem.*, *9*, 169–185, doi:10.1007/BF00052831.

Burrows, S. M., C. C. Hoose, U. Pöschl, and M. G. Lawrence (2013), Ice nuclei in marine air: Biogenic particles or dust?, *Atmos. Chem. Phys.*, *13*(1), 245–267, doi:10.5194/acp-13-245-2013.

Burton, S. P., R. A. Ferrare, M. A. Vaughan, A. H. Omar, R. R. Rogers, C. A. Hostetler, and J. W. Hair (2013), Aerosol classification from airborne HSRL and comparisons with the CALIPSO vertical feature mask, *Atmos. Meas. Tech.*, *6*, 1815–1858, doi:10.5194/amtd-6-1815-2013.

Choi, Y.-S., R. S. Lindzen, C.-H. Ho, and J. Kim (2010), Space observations of cold-cloud phase change, *Proc. Nat. Acad. Sci.*, *107*(25), 11,211–11,216, doi:10.1073/pnas.1006241107.

Connolly, P. J., O. Möhler, P. R. Field, H. Saathoff, R. Burgess, T. Choularton, and M. Gallagher (2009), Studies of heterogeneous freezing by three different desert dust samples, *Atmos. Chem. Phys.*, *9*, 2805–2824, doi:10.5194/acp-9-2805-2009.

Cozic, J., S. Mertes, B. Verheggen, D. J. Cziczo, S. J. Gallavardin, S. Walter, U. Baltensperger, and E. Weingartner (2008), Black carbon enrichment in atmospheric ice particle residuals observed in lower tropospheric mixed phase clouds, *J. Geophys. Res.*, *113*, D15209, doi:10.1029/2007JD009266.

Cziczo, D. J., K. D. Froyd, S. J. Gallavardin, O. Moehler, S. Benz, H. Saathoff, and D. M. Murphy (2009), Deactivation of ice nuclei due to atmospherically relevant surface coatings, *Environ. Res. Lett.*, *4*, 044013, doi:10.1126/science.1234145.

DeMott, P. J. (1990), An exploratory study of ice nucleation by soot aerosols, *J. Appl. Meteorol.*, *29*(10), 1072–1079, doi:10.1175/1520-0450(1990)0292.0.CO;2.

DeMott, P. J., K. Sassen, M. R. Poellot, D. Baumgardner, D. C. Rogers, S. D. Brooks, A. J. Prenni, and S. M. Kreidenweis (2003), African dust aerosols as atmospheric ice nuclei, *Geophys. Res. Lett.*, *30*(14), 1732, doi:10.1029/2003GL017410.

Diehl, K., and S. K. Mitra (1998), A laboratory study of the effects of a kerosene-burner exhaust on ice nucleation and the evaporation rate of ice crystals, *Atmos. Environ.*, *32*, 3145–3151, doi:10.1016/S1352-2310(97)00467-6.

Dymarska, M., B. J. Murray, L. Sun, M. L. Eastwood, D. A. Knopf, and A. K. Bertram (2006), Deposition ice nucleation on soot at temperatures relevant for the lower troposphere, *J. Geophys. Res.*, *111*, D04204, doi:10.1029/2005JD006627.

Eastwood, M. L., S. Cremel, M. Wheeler, B. J. Murray, E. Girard, and A. K. Bertram (2009), Effects of sulfuric acid and ammonium sulfate coatings on the ice nucleation properties of kaolinite particles, *Geophys. Res. Lett.*, *36*, L02811, doi:10.1029/2008GL035997.

Field, P. R., O. Möhler, P. Connolly, M. Krämer, R. Cotton, A. J. Heymsfield, H. Saathoff, and M. Schnaiter (2006), Some ice nucleation characteristics of Asian and Saharan desert dust, *Atmos. Chem. Phys.*, *6*(10), 2991–3006, doi:10.5194/acp-6-2991-2006.

Fornea, A. P., S. D. Brooks, J. B. Dooley, and A. Saha (2009), Heterogeneous freezing of ice on atmospheric aerosols containing ash, soot, and soil, *J. Geophys. Res.*, *114*, D13201, doi:10.1029/2009JD011958.

Forster, P., et al. (2007), Changes in atmospheric constituents and in radiative forcing, in *Climate Change 2007: The Physical Science Basis. Contribution of Working Group I to the Fourth Assessment Report of the Intergovernmental Panel on Climate Change*, Cambridge Univ. Press, Cambridge, U. K. and New York.

Friedman, B., G. Kulkarni, J. Beránek, A. Zelenyuk, J. A. Thornton, and D. J. Cziczo (2011), Ice nucleation and droplet formation by bare and coated soot particles, *J. Geophys. Res.*, *116*, D17203, doi:10.1029/2011JD015999.

Girard, E., J. P. Blanchet, and Y. Dubois (2005), Effects of arctic sulphuric acid aerosols on wintertime low-level atmospheric ice crystals, humidity and temperature at Alert, Nunavut, *Atmos. Res.*, *73*(1), 131–148, doi:10.1016/j.atmosres.2004.08.002.

Gorbunov, B., A. Baklanov, N. Kakutkina, H. L. Windsor, and R. Toumi (2001), Ice nucleation on soot particles, *J. Aerosol Sci.*, *32*(2), 199–215, doi:10.1016/S0021-8502(00)00077-X.

Hand, V., G. Capes, D. J. Vaughan, P. Formenti, J. M. Haywood, and H. Coe (2010), Evidence of internal mixing of African dust and biomass burning particles by individual particle analysis using electron beam techniques, *J. Geophys. Res.*, *115*, D13301, doi:10.1029/2009JD012938.

Hoose, C., and O. Möhler (2012), Heterogeneous ice nucleation on atmospheric aerosols: A review of results from laboratory experiments, *Atmos. Chem. Phys.*, *12*, 12531–12621, doi:10.5194/acp-12-9817-2012.

Hu, Y., D. Winker, M. Vaughan, B. Lin, A. Omar, C. Trepte, D. Flittner, P. Yang, S. Nasiri, and B. Baum (2009), CALIPSO/CALIOP cloud phase discrimination algorithm, *J. Atmos. Oceanic Technol.*, *26*(11), 2293–2309, doi:10.1175/2009JTECHA1280.1.

Isono, K., M. Komabayasi, and A. Ono (1959), The nature and origin of ice nuclei in the atmosphere, *J. Meteorol. Soc. Jpn.*, *37*, 211–233.

Kacenelenbogen, M., J. Redemann, M. A. Vaughan, A. H. Omar, P. B. Russell, S. Burton, R. R. Rogers, R. A. Ferrare, and C. A. Hostetler (2014), An evaluation of CALIOP/CALIPSO's aerosol-above-cloud detection and retrieval capability over North America, *J. Geophys. Res. Atmos.*, *119*, 230–244, doi:10.1002/2013JD020178.

Kanamitsu, M., W. Ebisuzaki, J. Woollen, S.-K. Yang, J. Hnilo, M. Fiorino, and G. L. Potter (2002), NCEP-DOE AMIP-II Reanalysis (R-2), *Bull. Am. Meteorol. Soc.*, *83*(11), 1631–1643, doi:10.1175/BAMS-83-11-1631.

Kim, S.-W., S. Berthier, J.-C. Raut, P. Chazette, F. Dulac, and S.-C. Yoon (2008), Validation of aerosol and cloud layer structures from the space-borne lidar caliop using a ground-based lidar in Seoul, Korea, *Atmos. Chem. Phys.*, *8*(13), 3705–3720, doi:10.5194/acp-8-3705-2008.

Knopf, D. A., and T. Koop (2006), Heterogeneous nucleation of ice on surrogates of mineral dust, *J. Geophys. Res.*, *111*, D12201, doi:10.1029/2005JD006894.

Koehler, K. A., S. M. Kreidenweis, P. J. DeMott, M. D. Petters, A. J. Prenni, and O. Möhler (2010), Laboratory investigations of the impact of mineral dust aerosol on cold cloud formation, *Atmos. Chem. Phys.*, *10*(23), 11,955–11,968, doi:10.5194/acp-10-11955-2010.

Liu, Z., M. Vaughan, D. Winker, C. Kittaka, B. Getzeich, R. Kuehn, A. Omar, K. Powell, C. Trepte, and C. Hostetler (2009), The CALIPSO lidar cloud and aerosol discrimination: Version 2 algorithm and initial assessment of performance, *J. Atmos. Oceanic Technol.*, *26*(7), 1198–1213, doi:10.1175/2009JTECHA1229.1.

Liu, Z., R. Kuehn, M. Vaughan, D. Winker, A. Omar, K. Powell, C. Trepte, Y. Hu, and C. Hostetler (2010), The CALIPSO cloud and aerosol discrimination: Version 3 algorithm and test results, *25th International Laser Radar Conference (ILRC)*, St. Petersburg, Russia, 5–9.

Lohmann, U., and K. Diehl (2006), Sensitivity studies of the importance of dust ice nuclei for the indirect aerosol effect on stratiform mixed-phase clouds, *J. Atmos. Sci.*, *63*(3), 968–982, doi:10.1175/JAS3662.1.

Lohmann, U., and C. Hoose (2009), Sensitivity studies of different aerosol indirect effects in mixed-phase clouds, *Atmos. Chem. Phys.*, *9*(22), 8917–8934, doi:10.5194/acp-9-8917-2009.

Lohmann, U., L. Rotstayn, T. Storelvmo, A. Jones, S. Menon, J. Quaas, A. M. L. Ekman, D. Koch, and R. Ruedy (2010), Total aerosol effect: Radiative forcing or radiative flux perturbation?, *Atmos. Chem. Phys.*, *10*(7), 3235–3246, doi:10.5194/acp-10-3235-2010.

Mahowald, N. M., M. Yoshioka, W. D. Collins, A. J. Conley, D. W. Fillmore, and D. B. Coleman (2006), Climate response and radiative forcing from mineral aerosols during the last glacial maximum, pre-industrial, current and doubled-carbon dioxide, *Geophys. Res. Lett.*, *33*, L20705, doi:10.1029/2006GL026126.

Mielonen, T., A. Arola, M. Komppula, J. Kukkonen, J. Koskinen, G. de Leeuw, and K. E. J. Lehtinen (2009), Comparison of CALIOP level 2 aerosol subtypes to aerosol types derived from AERONET inversion data, *Geophys. Res. Lett.*, *36*, L18804, doi:10.1029/2009GL039609.

Murray, B. J., D. O'Sullivan, J. D. Atkinson, and M. E. Webb (2012), Ice nucleation by particles immersed in supercooled cloud droplets, *Chem. Soc. Rev.*, *41*(19), 6519–6554, doi:10.1039/c2cs35200a.

Niemand, M., et al. (2012), A particle-surface-area-based parameterization of immersion freezing on desert dust particles, *J. Atmos. Sci.*, *69*, 3077–3092, doi:10.1175/JAS-D-11-0249.1.

Omar, A. H., et al. (2009), The CALIPSO automated aerosol classification and lidar ratio selection algorithm, *J. Atmos. Oceanic Technol.*, *26*(10), 1994–2014, doi:10.1175/2009JTECHA1231.1.

Omar, A., et al. (2010), Extinction-to-backscatter ratios of Saharan dust layers derived from in situ measurements and CALIPSO overflights during NAMMA, *J. Geophys. Res.*, *115*, D24217, doi:10.1029/2010JD014223.

Ou, S. S. C., et al. (2009), Retrievals of mixed-phase cloud properties during the National Polar-Orbiting Operational Environmental Satellite System, *Appl. Opt.*, *48*, 1452–1462, doi:10.1364/AO.48.001452.

Pappalardo, G., et al. (2010), EARLINET correlative measurements for CALIPSO: First intercomparison results, *J. Geophys. Res.*, *115*, D00H19, doi:10.1029/2009JD012147.

Petters, M. D., et al. (2009), Ice nuclei emissions from biomass burning, *J. Geophys. Res.*, *114*, D07209, doi:10.1029/2008JD011532.

Pruppacher, H. R., and J. D. Klett (1997), *Microphysics of Clouds and Precipitation*, Springer, New York.

Sassen, K., P. J. DeMott, J. M. Prospero, and M. R. Poellot (2003), Saharan dust storms and indirect aerosol effects on clouds: Crystal-face results, *Geophys. Res. Lett.*, *30*(12), 1633, doi:10.1029/2003GL017371.

Sesartic, A., U. Lohmann, and T. Storelvmo (2012), Bacteria in the ECHAM5-HAM global climate model, *Atmos. Chem. Phys.*, *12*(18), 8645–8661, doi:10.5194/acp-12-8645-2012.

Shupe, M. D., J. S. Daniel, G. D. Boer, E. W. Eloranta, P. Kollias, E. P. Luke, C. N. Long, D. D. Turner, and J. Verlinde (2008), A focus on mixed-phase clouds: The status of ground-based observational methods, *Bull. Am. Meteorol. Soc.*, *89*(10), 1549–1562, doi:10.1175/2008BAMS2378.1.

Storelvmo, T., J. E. Kristjánsson, and U. Lohmann (2008), Aerosol influence on mixed-phase clouds in CAM-Oslo, *J. Atmos. Sci.*, *65*(10), 3214–3230, doi:10.1175/2008JAS2430.1.

Targino, A., et al. (2009), Influence of particle chemical composition on the phase of cold clouds at a high-alpine site in Switzerland, *J. Geophys. Res.*, *114*, D18206, doi:10.1029/2008JD011365.

Tesche, M., U. Wandinger, A. Ansmann, D. Althausen, D. Müller, and A. H. Omar (2013), Ground-based validation of CALIPSO observations of dust and smoke in the Cape Verde region, *J. Geophys. Res. Atmos.*, *118*, 2889–2902, doi:10.1002/jgrd.50248.

Vali, G. (1985), Nucleation terminology, *Bull. Am. Meteorol. Soc.*, *66*(11), 1426–1427.

Winker, D. M., M. A. Vaughan, A. Omar, Y. Hu, K. A. Powell, Z. Liu, W. H. Hunt, and S. A. Young (2009), Overview of the CALIPSO mission and CALIOP data processing algorithms, *J. Atmos. Oceanic Technol.*, *26*, 2310–2323, doi:10.1175/2009JTECHA1281.1.

Winker, D. M., J. L. Tackett, B. J. Getzewich, Z. Liu, M. A. Vaughan, and R. R. Rogers (2013), The global 3-D distribution of tropospheric aerosols as characterized by CALIOP, *Atmos. Chem. Phys.*, *13*(6), 3345–3361, doi:10.5194/acp-13-3345-2013.

Yang, Z., A. K. Bertram, and K. C. Chou (2011), Why do sulfuric acid coatings influence the ice nucleation properties of mineral dust particles in the atmosphere?, *J. Phys. Chem. Lett.*, *2*(11), 1232–1236, doi:10.1021/jz2003342.

Zhang, Y., and G. R. Carmichael (1999), The role of mineral aerosol in tropospheric chemistry in East Asia—A model study, *J. Appl. Meteorol.*, *38*(3), 353–366.